INTERNATIONAL JOURNAL OF CLIMATOLOGY
Int. J. Climatol. **30**: 492–508 (2010)
Published online 15 April 2009 in Wiley InterScience
(www.interscience.wiley.com) DOI: 10.1002/joc.1914

RMetS
Royal Meteorological Society

Latitudinal height couplings between single tropopause and 500 and 100 hPa within the Southern Hemisphere

Adrián E. Yuchechen,[a,b]* Susana A. Bischoff[c] and Pablo O. Canziani[a,b]

[a] *Consejo Nacional de Investigaciones Científicas y Técnicas (CONICET), Argentina*
[b] *Equipo Interdisciplinario para el Estudio de Procesos Atmosféricos en el Cambio Global (PEPACG), Pontificia Universidad Católica Argentina (UCA), Argentina*
[c] *Departamento de Ciencias de la Atmósfera y los Océanos, Facultad de Ciencias Exactas y Naturales, Universidad de Buenos Aires (UBA), Argentina*

ABSTRACT: In order to provide further insights into the relationships between the tropopause and different mandatory levels, this paper discusses the coupling between standardized tropopause height anomalies (STHAs) and standardized 500-hPa and 100-hPa height anomalies (S5HAs and S1HAs, respectively) within the 'climatic year' for three sets of upper-air stations located approximately along 20 °S, 30 °S and 45 °S. Data used in this research consists in a radiosonde database spanning the period 1973–2007. The mandatory levels are supposed to be included in each radiosonde profile. The tropopause, on the other hand, is calculated from the significant levels available for each sounding using the lapse rate definition. After applying a selection procedure, a basic statistical analysis combined with Fourier analysis is carried out in order to build up the standardized variables. Empirical orthogonal functions (EOFs) in S-mode are used to get the normal modes of oscillation as well as their time evolution, for STHA/S5HA as well as for STHA/S1HA coupling, separately, within the aforementioned latitudes.

Overall, there are definite cycles in the time evolution associated with each EOF structure at all three latitudes, the semi-annual wave playing the most important role in most of the cases. Nevertheless, 20 °S seems to be the only latitude driven by diabatic heating cycles in the middle atmosphere. Certainly, EOF1 at this latitude has a semi-annual behaviour and seems to be strongly influenced by the tropical convection seasonality. Apparently, the convectively driven release of latent heat in the middle troposphere affects the time evolution of the EOF1 structure. By contrast, the vertical propagation of planetary waves is raised as a possible explanation for the EOF1 and EOF2 behaviour at latitudes beyond 20 °S, in view of the close connection existent between the semi-annual oscillation (SAO) and the reversion in the direction of the zonal wind.

KEY WORDS single tropopause; mandatory levels; coupling; Southern Hemisphere; EOF analysis

Received 26 September2007; Revised 3 March 2009; Accepted 8 March 2009

1. Introduction

There are many reasons to study the tropopause. Amid them is the need to understand stratosphere–troposphere exchange processes. Other processes taking place in its vicinity, e.g. wave breakings (Berrisford *et al*., 2007; Martius *et al*., 2007), are also relevant. Furthermore, tropopause height has been used as a tracer within the scope of global warming and climate change studies (e.g. Santer *et al*., 2003) and, more recently, to provide evidences of a widening of the tropical region (Seidel and Randel, 2007). Likewise, ozone changes can also significantly influence the tropopause (Santer *et al*., 2003). The tropopause is thus relevant in a number of atmospheric processes, making it necessary to understand the linkages between tropospheric as well as stratospheric processes in determining its evolution.

The World Meteorological Organization (WMO) defines the tropopause as 'the boundary layer between the troposphere and the stratosphere, where an abrupt change in lapse rate usually occurs'. The precise technical definition can be found, for instance, in WMO (1992), a definition regarded as the *thermal tropopause* or *lapse rate tropopause* (LRT). This definition also considers the presence of a second tropopause. LRT can then be used to obtain thermal tropopauses from radiosonde profiles. Strictly speaking, even though the exact location of LRT can only be obtained using significant levels, some algorithms estimate it from mandatory ones (e.g. Reichler *et al*., 2003; Zängl and Hoinka, 2001). Just the way WMO (1992) considers the presence of single as well as double tropopauses, even multiple tropopauses are expected to occur in certain situations and can be detected in a radiosonde profile. Therefore, within the LRT framework, the term 'tropopause' renders

* Correspondence to: Adrián E. Yuchechen, Equipo Interdisciplinario para el Estudio de Procesos Atmosféricos en el Cambio Global (PEPACG), Pontificia Universidad Católica Argentina (UCA), Facultad de Ciencias Agrarias, Capitán General Ramón Freire 183 – Office 45, C1426AVC – Ciudad Autónoma de Buenos Aires – Argentina.
E-mail: aey@uca.edu.ar

ambiguous. As a matter of fact, the tropopause should be viewed as a finite layer rather than as a transition surface (Bischoff *et al*., 2007; Pan *et al*., 2004).

The *dynamic tropopause* (DYN) is defined in terms of Ertel's potential vorticity (PV) (Ertel, 1942a, 1942b). A major issue when attempting to use PV with observational data is that the evaluation of the absolute vorticity needs to be accurate, something that cannot be accomplished for the extremely sparse Southern Hemisphere (SH) radiosonde network. Owing to the large stratospheric static stability, the PV magnitude increases upwards (e.g. Hartmann, 1977). This significant difference between the stratosphere and the troposphere can be exploited to define DYN as an isertelic surface, i.e. a PV isoline. However, the DYN definition remains arbitrary. Despite the fact that WMO (1986) defined DYN as the 1.6 potential vorticity units (PVU) surface for the Northern Hemisphere (NH) (similarly, -1.6 PVU in the SH), many authors have considered different values (e.g. Goering *et al*., 2001; Griffiths *et al*., 2000; Rood *et al*., 1997; Bush and Peltier, 1994; Rotunno *et al*., 1994; Hoerling *et al*., 1991) or even a variable latitude-dependant definition. Multiple tropopauses can also be found within the DYN framework anytime an isertelic surface is cut more than once by an imaginary vertical line. Many authors have assessed the similarities and differences between LRT and DYN. Amidst them, Wirth (2000) analysed the 'aspect ratio', i.e. hundredfold the vertical-to-horizontal ratio of PV anomalies, for upper-tropospheric balanced flow anomalies, concluding that LRT holds the same position and sharpness when the aspect ratio is either $\ll 1$ or $\gg 1$, whilst DYN does not. It is worth noting that the concept of *tropopause break* (TB) fits well within the LRT framework, while the concept of *tropopause folding* (TF) is used within the DYN framework. Both concepts are not separate entities though, and the location of TBs and TFs should coincide at least qualitatively in space as well as in time. Given this, from now on they are referred to as *multiple tropopause events* (MTEs), irrespective of the framework used.

The processes that lead to MTEs are not only tied to the subtropical jet (Baray *et al*., 2000; Kowol-Santen and Ancellet, 2000) but also to frontal system companion jets (Bischoff *et al*., 2007), cut-off cyclones (Wirth and Egger, 1999; Price and Vaughan, 1993), cyclogenesis (Appenzeller and Davies, 1992), synoptic and subsynoptic-scale interactions and processes (Appenzeller *et al*., 1996; Poulida *et al*., 1996; Uccellini *et al*., 1985) and wave breakings (Bradshaw *et al*., 2002; Postel and Hitchman, 1999; Lamarque *et al*., 1996). The schematic provided by Shapiro *et al*. (1987, cf. their Figure 17) for the NH suggests that the most important source for MTEs is connected to upper-level jets. A similar scenario probably holds for the SH, although many aspects of the tropopause studies are still lacking within this hemisphere.

The long-term position of the tropopause throughout the tropics can be depicted with a radiative-convective model (Schneider, 2007; Vallis, 2006, p 526; Barry and Carleton, 2001, p 121), in which vertical transports of heat prevent the lapse rate $\gamma = -\partial T/\partial z$ from exceeding a prescribed threshold, as long as deep convection is the dominant convective process. With regard to the extra-tropical regions, the lack of deep convection dominance complicates this straightforward picture. Notwithstanding, baroclinic eddies seem to play a central role in defining the extra-tropical tropopause height and upper troposphere/lower stratosphere (UTLS) behaviour (Canziani *et al*., 2008; Schneider, 2004; Haynes *et al*., 2001). In short, the location of the tropopause is most likely determined by instabilities, either convective (tropics) or baroclinic (extra-tropics). Thuburn and Craig (1997) noted that the height of the tropopause is strongly sensitive to the earth's surface temperature. A vivid example of their outcome arises when the tropopause over the Tropical Western Pacific Warm Pool (TWPWP) is considered. TWPWP is 'the region of the warmest sea surface temperature in the open oceans, which coexists with the largest annual precipitation and latent heat release in the atmosphere' (Webster and Lukas, 1992). According to Seidel *et al*. (2001), the tropopause reaches the coldest temperature records worldwide in the above-mentioned region. Nevertheless, Shimizu and Tsuda (2000) noted that the tropopause over Indonesia is even colder. Johnson (1986) analysed short-term variations of the TWPWP tropopause height and related them to deep convection. The latent heat released by convective-driven processes is critically important in determining the height of the tropopause. In other words, stability, which can be straightforwardly related to γ (e.g. Gates, 1961), plays an important role in its determination. The fact that there exists a proportional relationship between tropopause potential temperature and tropopause height and that the constant of proportionality involves stratospheric as well as tropospheric lapse rates (Juckes, 1994) stresses the importance of γ to the tropopause.

Canziani *et al*. (2008) recently discussed decadal variations in the SH extra-tropical UTLS, showing differing contributions to the state of this atmospheric region, depending on latitude and season. The behaviour of different variables at several mandatory levels has been also a major research topic for the SH. In particular, 500 hPa has been the object of many studies (e.g. Kidson and Sinclair, 1995; Ghil and Mo, 1991; Mo and Ghil, 1987; Trenberth, 1982, 1980, 1979) because it is considered a reference level for the middle troposphere. By contrast, research efforts addressing 100-hPa features are scarce. In spite of the existence of high-variability regions over the SH (Hoskins and Hodges, 2005; Nakamura and Shimpo, 2004; Berbery and Vera, 1996; Trenberth, 1991, 1981; Physick, 1981), the tropopause over these regions has received scant attention to date. Moreover, how each of these two mandatory levels behaves jointly with the tropopause as a function of latitude and season is still uncertain.

Unlike previous studies, the joint behaviour of the tropopause and these two mandatory levels is considered here. This is the main aim of the present research.

The radiosonde-derived thermal tropopause height and its coupling with the 500 and 100 hPa height along three latitudes in the SH is climatologically examined by means of the normal modes of oscillation. Normal modes in the atmosphere have been studied using different procedures (e.g. Brunet, 1994; Schnur *et al*., 1993), whereas an instructive theoretical approach to normal modes is presented in North (1984). Using empirical orthogonal function (EOF) analysis, the eigenvectors estimated from the correlation matrix are regarded as the normal modes of the system in the present research. In this respect, the present effort is entirely dedicated to the study of single tropopause events (STEs) and to present a description of the method employed. Additionally, a climatology-based explanation of why the number of MTEs increases southwards is presented. The present paper establishes the criteria and methodology necessary to perform a similar but complementary analysis referred to double tropopause events (manuscript in preparation).

An outline of this paper is as follows: Section 2 is devoted to data description and Section 3 describes the selection procedure and methodology. Results and discussion are presented in Section 4. Summary and concluding remarks appear in Section 5.

2. Data

Radiosonde data from the worldwide upper-air network are obtained from the dataset available at the Department of Atmospheric Science, College of Engineering, University of Wyoming (http://weather.uwyo.edu/). Each available sounding includes the following variables: pressure, height, temperature, dew point, mixing ratio, relative humidity, wind direction, wind intensity, potential temperature, equivalent potential temperature, virtual potential temperature as well as station information and sounding indices. Attention is focused on three different latitudes, with upper-air stations located approximately along 20 °S, 30 °S and 45 °S (Figure 1). Table I presents the list of these stations, along with other relevant information. Although the issue of data void regions is problematic in the SH, nine upper-air stations were taken to represent 20 °S and 45 °S, whilst ten stations were selected to do so for 30 °S. Radiosonde records at each station are selected depending on the most complete launching hour. The period spanned by each dataset as well as the percentage of available soundings at each station can be found in Table II. It can be seen from Table II that the records for those stations located in South America are most complete for 12Z, whereas the same is true for the remaining stations at 00Z. In general, those stations located in Australia and Oceania have more than 75% of available soundings. Also shown in Table II are the percentages of available data for 500 and 100 hPa as well as for detected tropopauses, as calculated from the total number of available soundings. The most important feature is that the chosen stations have more than 75% available data for both mandatory levels. As seen below, it is not casual that the lower percentages of detected tropopauses correspond to stations located beyond 45 °S.

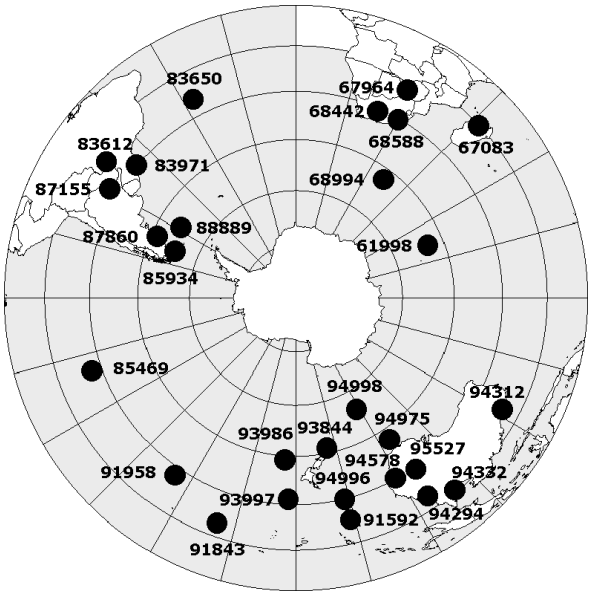

Figure 1. Location of the upper-air stations used in this research.

The tropopause-finding algorithm is as follows. Having separated significant and mandatory levels from each other for each available sounding, tropopauses are obtained from significant levels. Computations are carried out with the aid of a FORTRAN program with the capability to find up to five tropopauses. STEs as well as different MTEs are treated as being independent. Only six variables from each daily set of significant levels are kept, namely pressure, height, temperature, potential temperature, wind direction and wind intensity. Except for pressure, the same variables are kept for 500 and 100 hPa. For the whole analysis period, the number of tropopauses is accounted at each station and percentages of different tropopause events are calculated. These percentages are shown in Table III. STEs are dominant at all the stations, although some differences arise, depending on the latitude at which each station is found. In principle, MTEs percentages increase southwards. For instance, it is less than 10% over FMMI, while over FAME this percentage increases up to ≈25%. This can be straightforwardly related to the presence of high-variability regions, and is in complete agreement with the researches stating the fact that MTEs take place mostly in association with baroclinic zones (e.g. Staley, 1982, 1962, 1960). Indeed, the SH storm tracks (Hoskins and Hodges, 2005; Trenberth, 1991) are mainly located along the representative latitude for 45 °S considered here.

It is also convenient to know how many MTEs are not detected due to balloon burst. Mandatory levels included for almost all soundings are a good proxy for the balloon burst assessment at each station. The balloon burst level is close to the last reported mandatory level. The number of available mandatory levels between

Table I. Station information for the upper-air stations used in this research.

Station number	Station name	Station identifier	Latitude	Longitude	Elevation (m)
		20 °S			
67083*	Antananarivo	FMMI	18°47′S	47°28′E	1276
67964	Bulawayo	–	20°08′S	28°37′E	1344
83612	Campo Grande	SBCG	20°27′S	54°39′W	567
83650	Trindade	–	20°30′S	29°18′W	4
91592*	Noumea	NWWN	22°16′S	166°26′E	72
91843	Rarotonga	NCRG	21°12′S	159°48′W	7
94294*	Townsville	YBTL	19°15′S	146°45′E	9
94312*	Port Hedland	YPPD	20°22′S	118°37′E	9
YBMA	Mount Isa	YBMA	20°41′S	139°28′E	341
		30 °S			
68442	Bloemfontein	FABL	29°06′S	26°17′E	1354
68588*	Durban	FADN	29°57′S	30°57′E	14
83971	Porto Alegre	SBPA	30°00′S	51°11′W	3
85469*	Isla De Pascua	SCIP	27°09′S	109°26′W	41
87155*	Resistencia	SARE	27°27′S	59°02′W	52
91958*	Rapa	–	27°37′S	144°20′W	2
93997*	Raoul Island	NZRN	29°15′S	177°55′W	49
94578	Brisbane	YBBN	27°23′S	153°08′E	5
94996	Norfolk Island	YSNF	29°02′S	167°56′E	110
95527	Moree Mo	–	29°29′S	149°50′E	219
		45 °S			
61998*	Port-Aux-Francais	–	49°20′S	70°15′E	30
68994*	Marion Island	FAME	46°53′S	37°52′E	21
85934*	Punta Arenas	SCCI	53°00′S	70°20′W	33
87860*	Comodoro Rivadavia	SAVC	45°46′S	67°30′W	46
88889*	Mount Pleasant	EGYP	51°49′S	58°27′W	73
93844*	Invercargill	NZNV	46°24′S	168°18′E	4
93986*	Chatham Island	NZCI	43°57′S	176°33′W	48
94975*	Hobart	YMHB	42°50′S	147°30′E	27
94998*	Macquarie Island	YMMQ	54°30′S	158°57′E	8

The location of these stations can be found in Figure 1. The station identifier refers to the International Civil Aviation Organization (ICAO) code. Stations marked with an asterisk are included in Wallis (1998) as a subset of the Core Stations from the Comprehensive Aerological Dataset (CARDS).

850 and 10 hPa was accounted for in the total number of available soundings (cf. Table II). In summary, at almost all the stations along 20 °S (30 °S and 45 °S), that number presents a dramatic decrease upwards of 100 hPa (50 hPa) (results not shown). It can be inferred from these results that MTEs can rarely be detected using radiosonde data along 20 °S. The combination of the level of balloon burst and the location of high-variability regions would appear to suggest a plausible explanation on why the number of MTEs increases southwards. It is interesting to note from Table III that percentages of STEs at all the stations located in 20 °S are over 75%, and that for MTEs for most, but not all, of the stations located in 45 °S are over 25%, in accordance with the above-exposed arguments. It is worth mentioning that the percentage of MTEs is over 10% for all the stations beyond 20 °S. The greatest MTE percentage is not present over the southernmost latitude, but over Moree Mo, located in 30 °S. Sinclair (1995, 1994) showed that the region where this station is found is one of the most cyclogenetically active in the SH, particularly in winter. Similar results at 300 hPa can be found in Inatsu and Hoskins (2004). The combination of either Sinclair's or Inatsu and Hoskins' results along with the ones presented in this work highlight the fact that MTEs are expected to occur at high-variability regions. Furthermore, the minimum number of STEs is accounted over SAVC, a southernmost latitude station also presenting the highest record of triple as well as quadruple tropopause events (not discernable from Table III). These kinds of results suggest the fact that local processes critically influence the tropopause. Nevertheless, aside from the influence of local processes, the above-mentioned rule of thumb, which is just an outline of the real scenario, is a very good approximation.

3. Methodology

After obtaining the tropopauses at each station, a selection procedure is applied to each variable in order to discard potentially erroneous values. Wind direction is excluded, nevertheless, because *a priori* any value

Table II. Percentage of available soundings, indicated for the most complete launching hour at each station, along with the percentage of available data for tropopause, 500 hPa and 100 hPa as obtained from the number of available soundings. 'Tropopause' encompasses single as well as multiple detected tropopauses.

Station	Launching hour	Time period	Percentage of available data			
			Soundings	Tropopause	500 hPa	100 hPa
61998	12Z	07 May 1973–31 December 2007	68.45	**87.13**	**80.85**	**75.84**
67083	00Z	25 January 1973–20 April 2007	66.21	47.34	**78.63**	69.16
67964	00Z	07 May 1974–27 April 1999	**75.67**	43.30	**86.57**	**78.21**
68442	12Z	03 January 1973–29 December 2007	70.08	64.48	**92.81**	**86.48**
68588	00Z	01 January 1973–31 December 2007	**86.86**	74.13	**97.33**	**93.03**
68994	00Z	16 January 1973–31 December 2007	**84.61**	**83.40**	**97.40**	**90.64**
83612	12Z	05 January 1973–31 December 2007	69.65	47.59	**95.20**	**86.59**
83650	12Z	02 January 1973–23 December 2007	49.20	63.15	**88.78**	**76.98**
83971	12Z	03 January 193–31 December 2007	**86.91**	**79.93**	**96.89**	**89.21**
85469	00Z	25 January 1973–31 December 2007	47.85	**76.69**	**94.77**	**88.29**
85934	12Z	22 July 1976–31 December 2007	**86.24**	**81.54**	**96.67**	**85.81**
87155	12Z	04 January 1973–31 December 2007	**77.72**	**78.09**	**89.63**	**81.57**
87860	12Z	02 January 1973–31 December 2007	73.61	**87.96**	**93.23**	**83.26**
88889	12Z	07 April 1988–31 December 2007	**81.63**	**97.40**	**89.31**	**96.53**
91592	00Z	01 January 1973–31 December 2007	**92.59**	**83.73**	**96.19**	**91.53**
91843	00Z	10 August 1974–31 December 1989	**87.91**	63.58	**96.44**	**86.65**
91958	00Z	02 January 1973–1 December 2007	**89.81**	**75.63**	**95.77**	**79.89**
93844	00Z	01 January 1973–29 September 2007	**80.65**	**86.56**	**96.17**	**89.87**
93986	00Z	01 January 1973–29 September 2007	74.31	**90.60**	**94.81**	**89.64**
93997	00Z	01 January 1973–05 December 2007	52.32	**82.39**	**95.33**	**87.46**
94294	00Z	01 January 1973–31 December 2007	**90.94**	**79.73**	**95.96**	**94.58**
94312	00Z	01 January 1973–31 December 2007	**90.06**	**75.31**	**92.33**	**92.50**
94332	00Z	15 December 1976–31 December 2007	**89.39**	**82.66**	**97.34**	**95.14**
94578	00Z	01 January 1973–31 December 2007	**92.04**	**83.86**	**95.71**	**95.61**
94975	00Z	01 January 1973–31 December 2007	**90.18**	**93.25**	**96.72**	**94.92**
94996	00Z	01 January 1973–31 December 2007	**86.31**	67.84	**94.58**	**92.98**
94998	00Z	01 January 1973–31 December 2007	**89.17**	**91.47**	**95.62**	**91.85**
95527	00Z	16 January 1973–31 December 2007	**89.91**	**92.55**	**99.61**	**98.22**

Bold face type indicates a minimum of 75% of available data. Please note that the time period spanned by the datasets is not the same at all the stations.

ranging from 0 to 360 is allowed. The selection procedure determines that if the departure, in absolute value, of any variable from its monthly mean exceeds 2 units of monthly standard deviation, then that tropopause is discarded. If any wind variable is missing, the companion variables are nevertheless kept. Given that wind is one of the most frequently missing variables, this criterion is to avoid discarding all the remaining variables at relevant levels, particularly the tropopause. Those tropopauses whose associated variables simultaneously satisfy the selection procedure are kept. The same holds for 500 and 100 hPa. Table IV presents the percentage of rejected data after the selection procedure was applied. From the outcome of this selection procedure, Bulawayo (Trindade, FADN) has the best records for tropopause (500 hPa, 100 hPa), whilst FAME (NWWN, EGYP) has the worst. The selection procedure is also helpful in estimating the monthly variability at each level. For instance, the aforementioned result stresses the fact that single tropopause events over Bulawayo are the ones presenting the least variability amongst the single tropopause datasets considered.

The mean annual cycle or 'climatic year' is built up by calculating the mean height values for each of the 366 days. Table II provides the period spanned at each station for this averaging process. If missing values occur, they are estimated by linear interpolations. Only data that comply with the selection procedure (cf. Tables II and IV) for tropopause as well as for both mandatory levels are included in this climatology. As an example, mean height values throughout the climatic year over YMHB are presented in Figure 2. The annual cycle shown is an example of all stations considered because an annual behaviour is always present to a greater or a lesser degree. In order to extract as much deterministic behaviour as possible, time series are Fourier analysed, thereafter building anomalies as the departures from the combined grand time mean and those harmonics explaining each more than 10% of the total variance. This is done for each time series at each station.

The EOF method is carried out using the S-mode correlation matrix (see, e.g. Richman, 1986). The term EOF is used here to describe each eigenvector extracted from the correlation matrix, whilst the time-evolving

Table III. Percentage of tropopause events as calculated from the total number of available tropopause data (cf. Table II).

Station	Percentage of tropopause events		
	Single	Double	Other
61998	**81.38**	16.69	1.93
67083	**93.82**	6.10	0.08
67964	**94.55**	5.45	0.00
68442	69.87	**28.99**	1.14
68588	66.95	**31.77**	1.26
68994	72.57	**25.25**	2.18
83612	**89.52**	10.34	0.14
83650	**86.55**	13.30	0.15
83971	64.73	**33.37**	1.90
85469	68.26	**31.12**	0.62
85934	65.00	**25.85**	9.15
87155	**76.72**	22.06	1.22
87860	54.37	**32.27**	**13.35**
88889	58.56	**31.11**	**10.33**
91592	**93.66**	6.30	0.04
91843	**92.01**	7.89	0.10
91958	**78.76**	20.93	0.30
93844	74.47	22.72	2.81
93986	**78.16**	20.01	1.83
93997	74.65	24.59	0.76
94294	**94.00**	5.85	0.15
94312	**94.40**	5.56	0.05
94332	**93.83**	6.13	0.04
94578	**76.26**	22.95	0.79
94975	64.25	**29.09**	6.66
94996	**77.25**	22.39	0.36
94998	**83.02**	14.54	2.44
95527	63.12	**34.47**	2.40

Bold face type indicates a minimum of 75% for single tropopause events, a minimum of 25% for double tropopause events and a minimum of 10% for tropopause events other than single and double.

Table IV. Percentage of rejected data after applying the selection procedure.

Station	Percentage of rejected data		
	Single tropopause	500 hPa	100 hPa
61998	10.60	**9.28**	**9.02**
67083	**7.64**	**4.84**	**6.27**
67964	**6.30**	**6.41**	**6.89**
68442	**8.40**	**8.14**	**6.07**
68588	**8.46**	**7.19**	**5.07**
68994	14.00	**9.84**	**8.15**
83612	**9.02**	**6.93**	**6.41**
83650	**7.83**	**4.27**	**6.59**
83971	**8.80**	**7.64**	**8.65**
85469	10.33	**7.45**	**8.13**
85934	10.84	**8.24**	**7.99**
87155	**8.42**	**5.48**	**6.60**
87860	12.58	**8.28**	**6.97**
88889	10.58	**9.53**	11.46
91592	**8.21**	10.36	**8.81**
91843	**8.37**	**8.47**	**9.11**
91958	**9.72**	**9.48**	10.03
93844	11.36	10.00	**7.48**
93986	10.44	**7.62**	**7.06**
93997	**9.26**	**7.62**	**6.75**
94294	**6.91**	**6.75**	**6.25**
94312	**8.01**	**7.63**	**7.58**
94332	**7.50**	**9.62**	**8.27**
94578	10.37	**8.78**	**7.90**
94975	11.50	**9.70**	**8.44**
94996	10.20	**7.39**	**6.64**
94998	**9.81**	**9.27**	**9.44**
95527	**9.66**	10.35	10.16

Percentages are calculated from the total number of available data (cf. Table II). Bold face type indicates less than 10% of rejected data.

coefficients associated with each EOF (cf. Kutzbach, 1970, 1967) are referred to as *factor scores* (FSs), or simply *scores*. EOFs are mutually orthogonal in the space domain in a similar fashion that the scores are orthogonal with each other in time, playing the role of 'time-weighted' coefficients for each EOF.

The method allows the analysis of the simultaneous coupling between the tropopause, 500 and 100 hPa time series. Nevertheless, the 500 hPa/100 hPa coupling masks the other two as the tropopause possesses a considerable variability. In order to avoid this, the coupling between the tropopause and each mandatory level is studied separately. Matrix $\mathbf{Z}$ is built for each latitude so that it has 366 columns. Likewise, the number of rows is twice the number of upper-air stations per latitude. The upper half of the rows includes the standardized tropopause height departures throughout the climatic year, one row per station. The standard deviation value at each row equals 1. The same holds for the lower half of the rows, but including 500 or 100 hPa data independently. Eigenvectors are extracted from the correlation matrix, namely $\mathbf{R} = \mathbf{Z}\mathbf{Z}^{\mathbf{T}}$, with the aid of a foolproof method such as the Jacobi transformations (e.g. Golub and VanLoan, 1989).

4. Results and discussion

Before proceeding, it is necessary to take into account one important aspect of EOFs. According to North *et al*.'s rule of thumb (North *et al*., 1982), the 'effective degeneracy' is present when two eigenvalues are close to each other. Following this, presenting all the extracted EOFs is not necessary at all. In most of the cases, it is sufficient to focus on the study of the leading two or three modes. Additionally, following Quadrelli *et al*. (2005), when North *et al*.'s rule of thumb holds for any pair of eigenvalues, the corresponding EOFs are reliable ones. Figure 3(a)) shows EOF1 and EOF2 for the coupling between standardized tropopause height anomalies (STHAs) and standardized 500-hPa height anomalies (S5HAs). This coupling is referred to as *T5C* hereinafter. EOF1 (EOF2) accounts for ≈16% (≈10%) of the total explained variance. It can be seen from Figure 3(a)) that STHAs are in opposite phase with the corresponding S5HAs for more than half of the

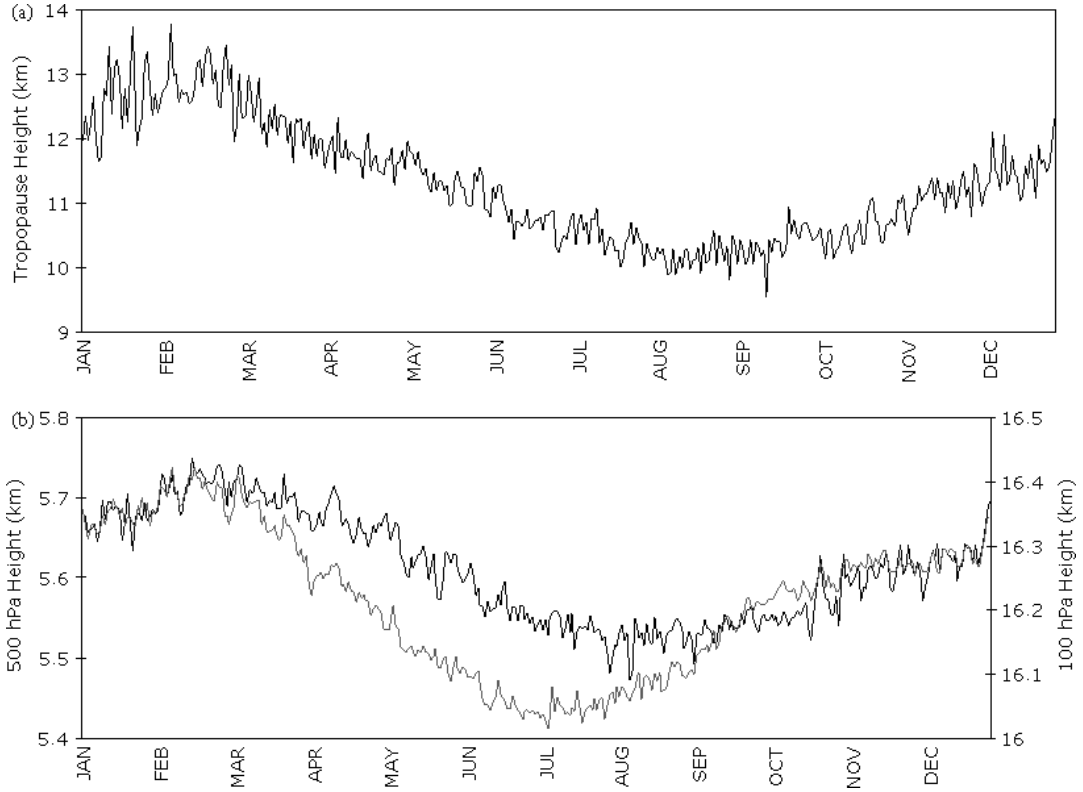

Figure 2. Mean heights for the 'climatic year' at YMHB: (a) single tropopause; (b) 500 hPa (black) and 100 hPa (grey).

stations. Furthermore, there is an important feature for those stations located within or in the vicinities of the TWPWP. Defining T5T as STHA-S5HA, i.e. some kind of thickness, it can be seen that the values reached by T5T at these stations are prominent. A plausible explanation for this is presented below. On the other hand, EOF2 shows that STHA and S5HA are in phase for most of the stations.

The coupling between STHAs and the standardized 100-hPa height anomalies (S1HAs) are referred to as *T1C*. EOF1 and EOF2 for T1C are presented in Figure 3(b)). They account for ≈14% and ≈9% of the total explained variance, respectively. EOF1 reveals that the absolute value of STHA−S1HA (T1T) is smaller than T5T for most of the stations, as it should, because 100 hPa has been widely used as a proxy for the tropopause by many authors (Mote *et al.*, 1996; Newell and Gould-Stewart, 1981). Therefore, the long-term position of the single tropopause for those stations lying throughout 20 °S is broadly located at 100 hPa and, at least with respect to height, the aforementioned stations can be considered as tropical ones. With regard to EOF2, STHA and S1HA are in opposite phase for some stations located in the vicinity of TWPWP, resembling somewhat the T5C EOF1 behaviour. On the contrary, anomalies are in phase for the stations located west of the Greenwich Meridian.

In view of the proximity of the tropical tropopause to 100 hPa, calculations for this latitude were also carried out for 70 and 50 hPa in order to avoid the potential overlapping of both surfaces as well as to ensure the coupling of the tropopause with a level located well in the stratosphere. EOF1 and EOF2 for the coupling between STHAs and standardized 70- and 50-hPa height anomalies are presented in Figure 3(c) and (d)), respectively. Results concerning EOF1 are not much different than those for T1C. By contrast, a clearer pattern is obtained for EOF2. These results are in agreement with the studies suggesting that the tropopause height is well correlated with the temperature in the lower stratosphere (e.g. Seidel and Randel, 2006).

With regard to the TWPWP region, an interesting result is that, for EOF1, standardized anomalies are out of phase for T5C but in phase for T1C, suggesting that there is a regional process taking place between 500 hPa and the tropopause but not extending into the stratosphere. For a better understanding of this process, it is necessary to analyse the time evolution of each EOF as given by $\mathbf{Z} = \mathbf{EC}(t)$. In other words, each EOF is fixed and the time evolution is given by the scores. Scores time series for EOF1 and EOF2 at 20 °S are presented in Figure 4. A Fourier analysis for the T5C FS1 (FS2) time series shown in Figure 4(a)) reveals that the leading harmonic is the second – semi-annual – (third – terannual –), accounting for ≈56% (≈26%) of the total explained variance. The matter is somewhat different regarding T1C (Figure 4(b)) because there are no leading harmonics for FS1. Instead, most of the explained variance is distributed among the first ten harmonics. With regard to FS2, the leading harmonic is the second one and accounts for ≈32% of the total explained variance. With regard to tropopause/70 hPa

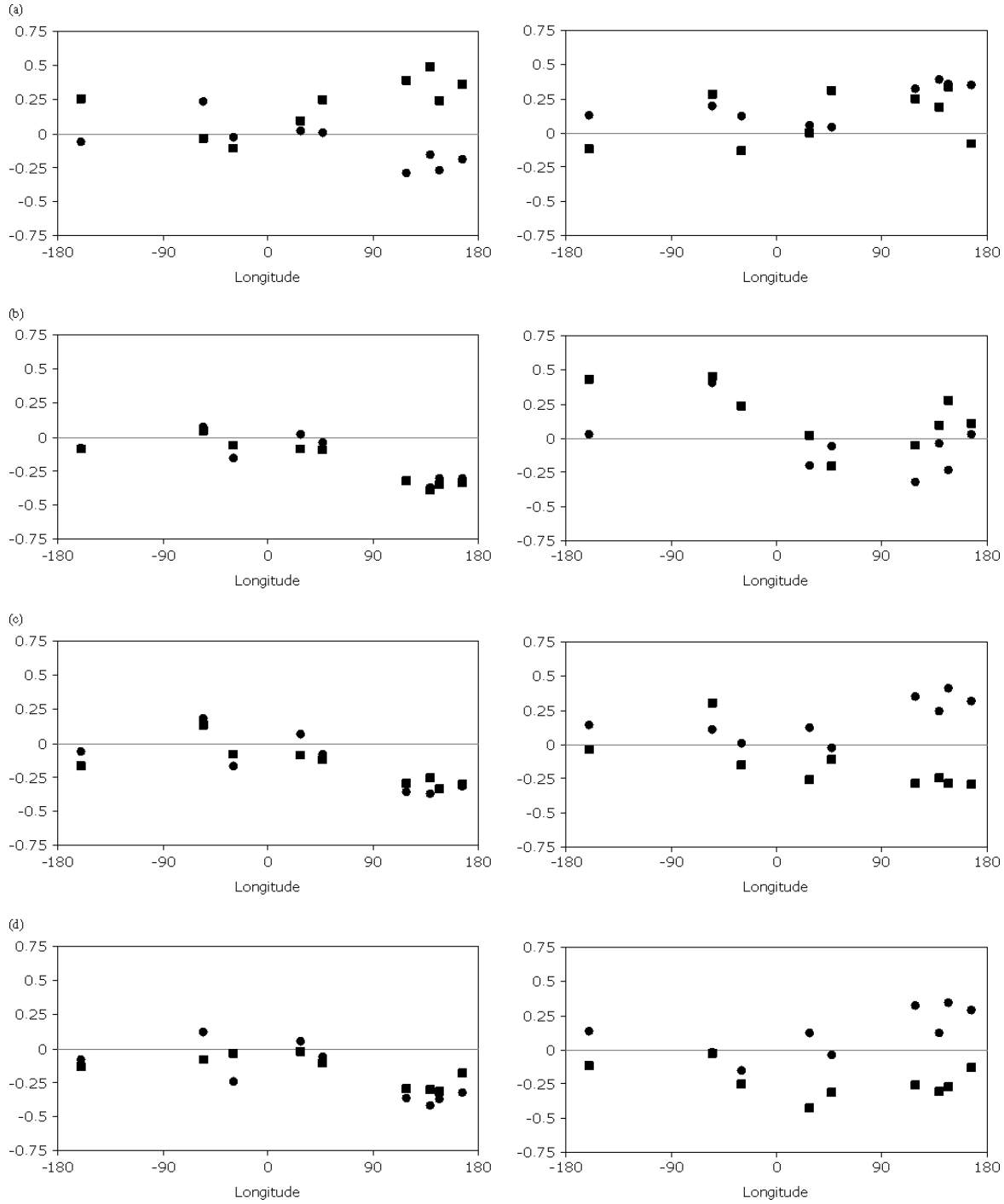

Figure 3. Normal modes for the coupling at 20 °S between standardized tropopause height anomalies and standardized height anomalies for (a) 500 hPa; (b) 100 hPa; (c) 70 hPa; (d) 50 hPa. EOF1 (EOF2) is presented in the left (right) panel. Circles (squares) represent the tropopause (mandatory level).

coupling, the leading harmonics for FS1 are the second and the third ones, accounting for ≈18% and ≈15% of the total explained variance, respectively, while for FS2 the leading harmonic is the third one, accounting for ≈27% of the total explained variance. With respect to tropopause/50 hPa coupling, the second and third harmonics are the leading ones for FS1 (≈20% and ≈12%, respectively), whilst the second harmonic is the most important (≈20%) for FS2. Explained variances aside, it is evident from a comparison of Figure 4(c) and (d)) that the time evolution of FS1 for 70 and 50 hPa is very similar, and that the same holds for FS2. These results highlight the fact that 70 hPa is a good alternative to avoid the 100-hPa issues previously raised.

Despite the presence of a leading semi-annual harmonic in T5C FS1 (cf. Figure 4(a)), which in principle denotes a reversion in the associated EOF1 structure twice a year, FS1 values are strictly negative only within summer. The situation is somewhat different during winter because FS1 values are strictly negative early in this

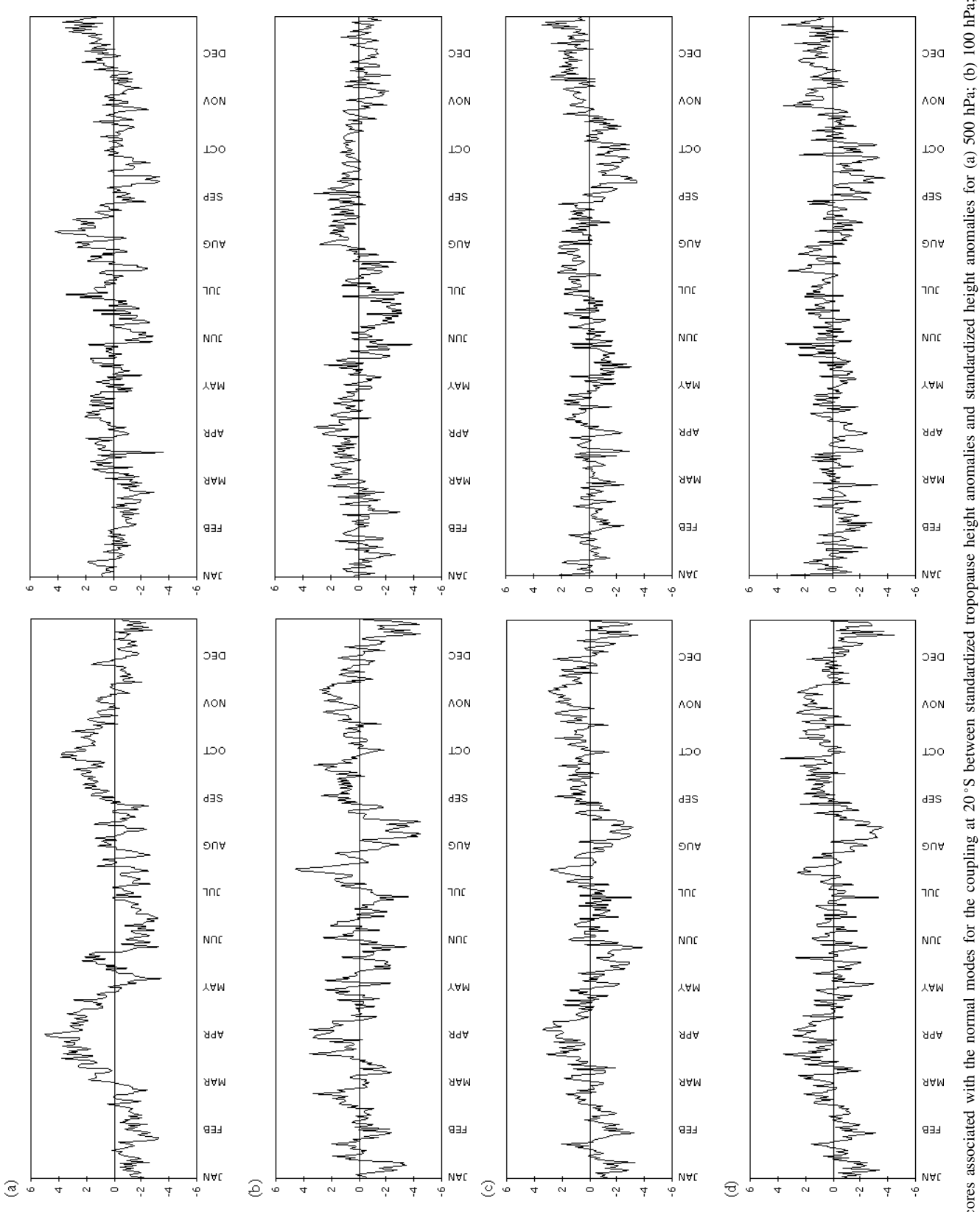

Figure 4. Scores associated with the normal modes for the coupling at 20 °S between standardized tropopause height anomalies and standardized height anomalies for (a) 500 hPa; (b) 100 hPa; (c) 70 hPa; (d) 50 hPa. FS1 (FS2) is presented in the left (right) panel.

season only; by contrast, in late winter, FS1 values oscillate from positive to negative, i.e. the so-called 'flip-flop' behaviour arises. By definition, an EOF pattern is said to be in direct (indirect) mode anytime its associated evolution coefficient is positive (negative). Flip-flop behaviour is therefore a somewhat sudden transition from one mode to its opposite counterpart. EOF1 structure is in correspondence with a direct mode during fall and spring. With regard to T5C FS2, the associated EOF2 pattern has a well-defined behaviour only within early summer (direct mode) and late summer (indirect); flip-flop behaviour takes place throughout the rest of the year. Both associated spatial structures are flip-flop behaved all year long in regard to T1C (cf. Figure 4(b)), although sign-like periods are more distinguishable for FS2. Notwithstanding, the orthogonal constraint must hold regardless the behaviour of each score.

A noteworthy feature of T5C FS1 is that it reaches negative values all summer long, which seemingly can be related to heating sources as follows. Yanai and Tomita (1998) present the seasonal variability of the heat source between 50 °N and 50 °S. Particularly interesting is their Figure 1, despite the fact that the heat source is vertically integrated throughout the troposphere. Within the TWPWP, they found that the heat source peaks during SH summer and winter, maximum values taking place south (north) of the Equator for the former (latter) season. On the other hand, owing to the time evolution of FS1 (cf. Figure 4(a)), T5T is positive during summer, in coincidence with the maximum stage of the heating in the troposphere, and during winter, although certain flip-flop behaviour is embedded in the time series for this latter case. It can be argued at this point that the use of vertically integrated heat sources is somewhat inappropriate because they include the total column of air. Figure D28 (ERAD28 henceforth) from the ERA-40 Atlas (Kållberg *et al*., 2005, ERA-40 henceforth) provides a zonally averaged picture of diabatic heating, showing that over 20 °S the core of heating is located just in the vicinity of 500 hPa only for the SH summer. In fact, this is the only season in which there is a net heating for the whole middle troposphere at the aforementioned latitude. Therefore, EOF1 winter flip-flop behaviour as well as the reversed structure during fall and spring seemingly responds to a net cooling of the middle atmosphere, suggesting that T5C EOF1 at 20 °S might be driven by diabatic heating processes in the middle troposphere.

Moving into 30 °S, the first two EOFs for T5C as well as for T1C are shown in Figure 5. Likewise, the scores time series for these structures are shown in Figure 6. The explained variances are ≈17% and ≈13% for T5C. EOF1 shows that STHAs and S5HAs are in phase at all the stations. EOF2 somewhat resembles the T5C EOF1 structure for 20 °S in the sense that those stations located closer to the date line present extreme T5T values. A Fourier analysis of FS1 and FS2 time series reveals that the leading harmonic is the second one in both cases, accounting for ≈63% and ≈53% of the total explained variance, respectively. The semi-annual wave is clearly dominant in these time series. Related to this, the EOF1 structure is in direct mode in early and mid-fall, mid-winter and mid-spring; whereas indirect mode prevails in late fall/early winter, and late spring/early summer. On the other hand, the EOF2 structure is in direct (indirect) mode in late fall and mid-spring (winter), whereas

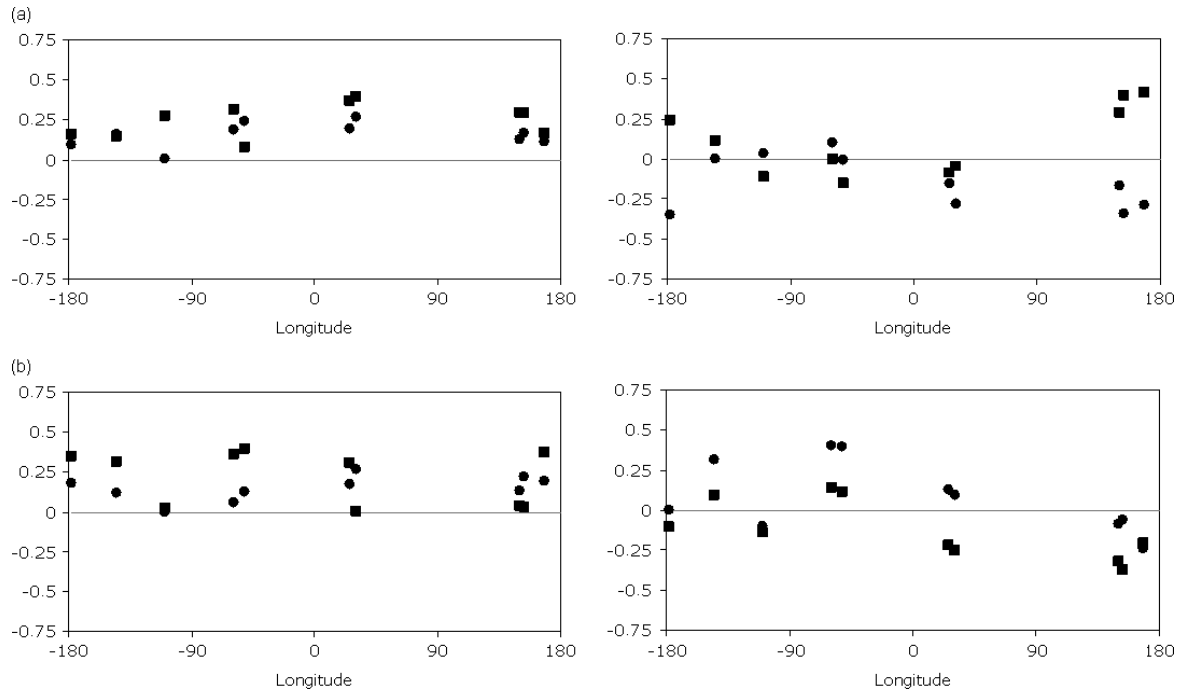

Figure 5. Normal modes for the coupling at 30 °S between standardized tropopause height anomalies and standardized height anomalies for (a) 500 hPa; (b) 100 hPa. EOF1 (EOF2) is presented in the left (right) panel. Circles (squares) represent the tropopause (mandatory level).

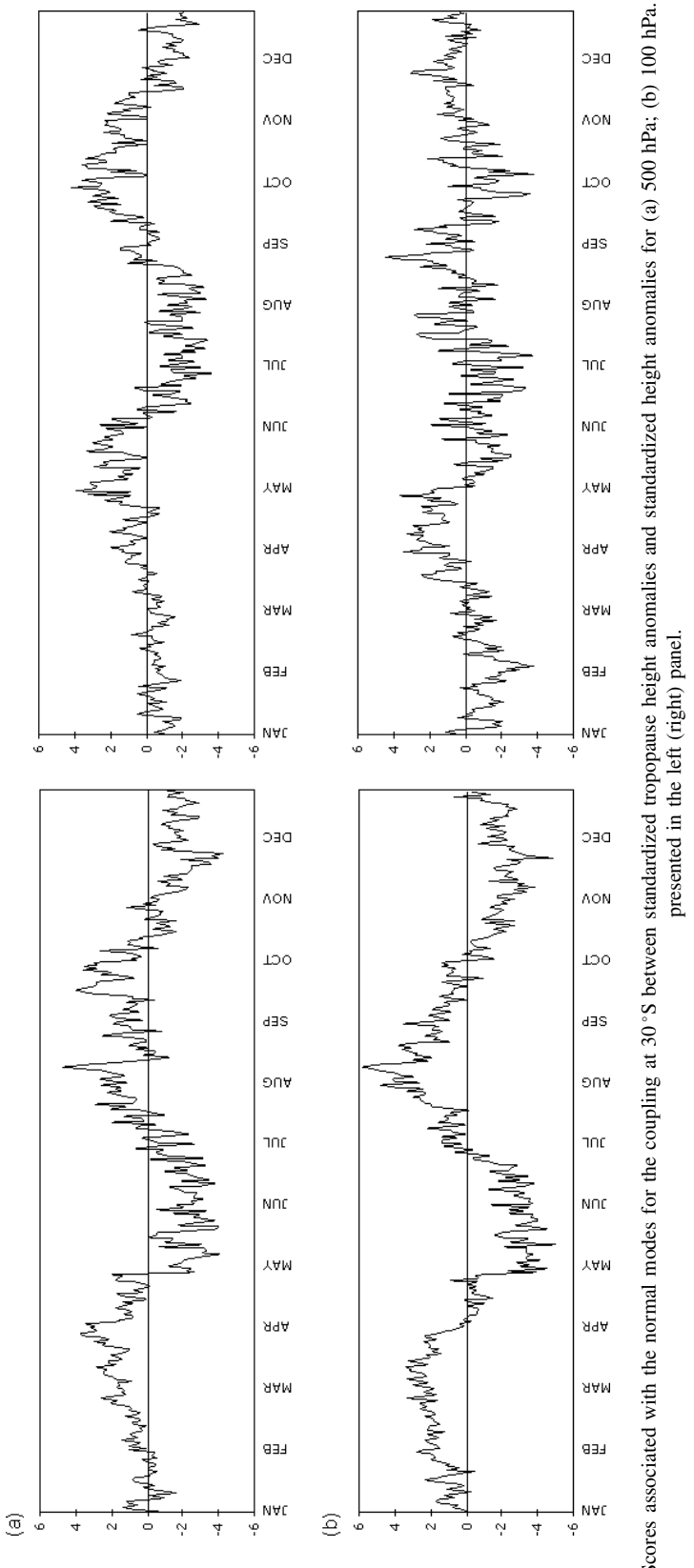

Figure 6. Scores associated with the normal modes for the coupling at 30 °S between standardized tropopause height anomalies and standardized height anomalies for (a) 500 hPa; (b) 100 hPa. FS1 (FS2) is presented in the left (right) panel.

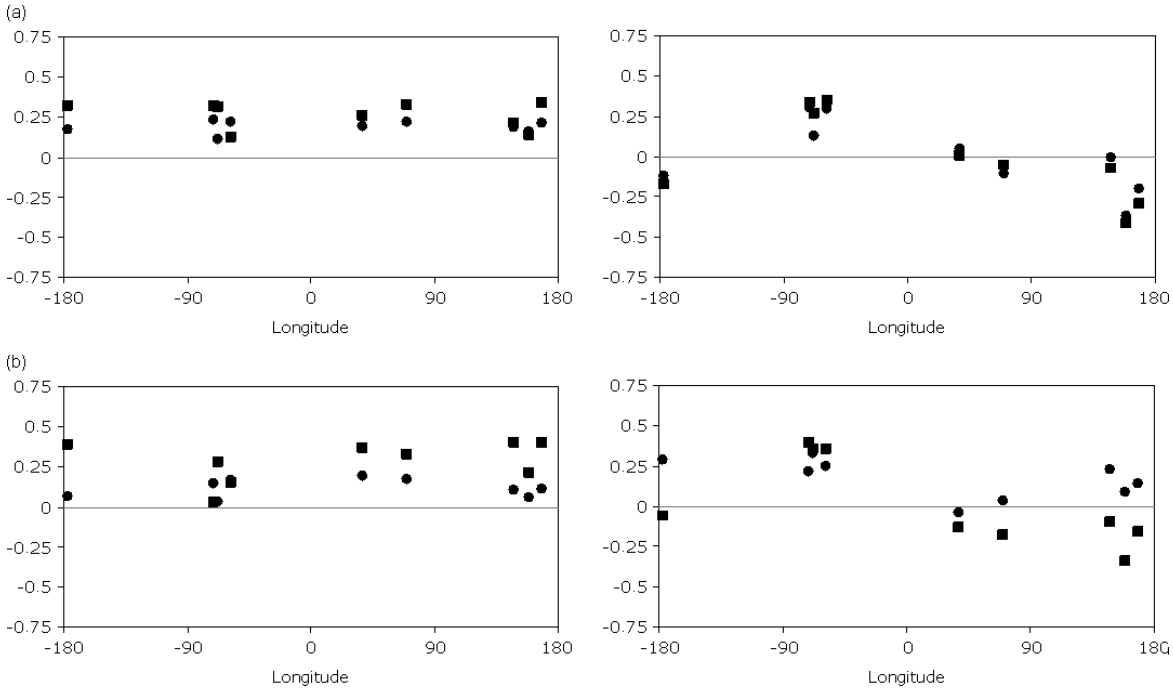

Figure 7. As in Figure 5 but for 45 °S.

summer is flip-flop behaved. An attempt to explain these results using ERAD28 is unsuccessful because the zonal mean heating over 30 °S presents no significant cycles between the tropopause and 500 hPa. Therefore, it cannot be concluded whether EOF1 or EOF2 time evolution is attributable to diabatic heating cycles. Nevertheless, recall that ERAD28 arises as a zonal average, and that the time evolution of the structures shown here is possibly affected by regional effects. Figure 5(b)) shows the first two EOF structures for T1C. Their explained variances are ≈24% and ≈11%. STHAs and S1HAs are quite in phase at almost all the stations for EOF1. Aside from the African stations, the same holds for EOF2. The presence of a semi-annual cycle in FS1 (cf. Figure 6(b)) is outstanding, which is also revealed by a striking 83% of explained variance after Fourier analysing this time series. On the other hand, the third harmonic (terannual wave) is the leading one for FS2, accounting for almost 32% of the total explained variance. Following this, the EOF1 structure reverses twice a year, being in direct (indirect) mode in summer and winter (fall and spring), and the flip-flop behaviour is present only for season-to-season transitions. With regard to EOF2, the flip-flop behaviour is present all year long except for mid-fall. Quadrelli *et al.*'s and North *et al.*'s rules of thumb are applicable for the two EOF sets corresponding to this latitude.

With regard to 45 °S, Figure 7 comprises the first two EOFs for T5C as well as for T1C, and the associated scores for these structures are presented in Figure 8. With regard to the spatial patterns, explained variances for T5C are ≈20% and ≈13%. EOF1 structure is not much different than the one for 30 °S (cf. Figure 5(a) because anomalies are all positive. With regard to EOF2, anomalies are also present in phase, although the sign reverses within the central domain, i.e. for those stations located in the vicinities of the southern tips of South America and Africa. The leading cycle in FS1 (cf. Figure 8(a)) is semi-annual, accounting for almost 51% of the total explained variance, implying a reversal of the EOF1 structure twice a year. Roughly speaking, it is in direct (indirect) mode in late summer/early fall and late winter/early spring (early winter and late spring/early summer). With regard to FS2, there is practically no leading harmonic at all because the 19th is the leading one, accounting for less than 10% of the total explained variance. Spatial explained variances are ≈27% and 11% for T1C (Figure 7(b)). The EOF1 pattern resembles that of the T5C counterpart as anomalies at all stations are positive. Anomalies are in opposite phase mainly close to the date line for EOF2. After Fourier analysing the FS1 time series (cf. Figure 8(b)), ≈67% of the explained variance is retained by the semi-annual wave, implying that the EOF1 structure reverses twice a year, being in direct (indirect) mode in early fall and late spring (early summer and late fall/early winter). With regard to FS2, the leading harmonic is also the second one, accounting for almost 30% of the total explained variance. Nonetheless, the flip-flop behaviour is present almost all year long, perhaps with an exception in mid-winter when the structure holds in direct mode for a short period. At 45 °S, significant cycles in diabatic heating are present, albeit below 600 hPa (cf. ERAD28). Therefore, an attempt to use ERAD28 to explain the foregoing results for 45 °S would be unsuccessful again. Finally, Quadrelli *et al.*'s and North *et al*'s rules of thumb can be applied to the EOF sets presented for this latitude.

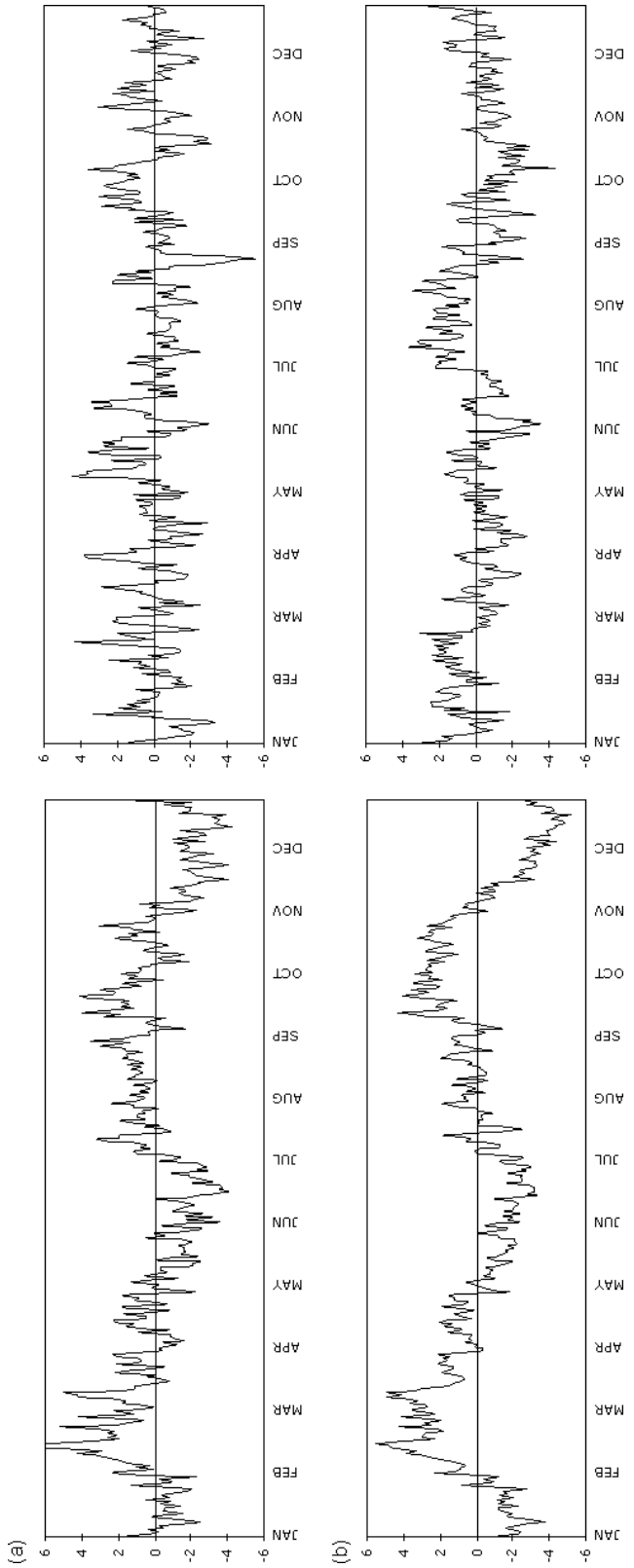

Figure 8. As in Figure 6 but for 45°S.

5. Summary

In spite of the fact that the radiosonde dataset at some stations used in this research did not cover the entire period of analysis well (Table II), the amount of available information is good enough to ensure statistical robustness alongside a well-set climatology. The normal modes of oscillation for the coupling between tropopause height anomalies and 500- or 100-hPa height anomalies within the 'climatic year' for three different latitudes, namely 20 °S, 30 °S and 45 °S, have been presented, along with their time evolution. The EOF method provides a convenient way to expand gridded time series as a linear combination of the normal modes, i.e. the EOFs, with time-varying coefficients, i.e. the scores, through the relation $\mathbf{Z} = \mathbf{EC}(t)$. Usually, the combination of the first two or three EOFs is quite enough to get the most important cycles. Quite often, in geophysical systems, higher-order EOFs are not considered because they account for a little percentage of the total explained variance.

The leading normal modes for the coupling between standardized tropopause height anomalies and standardized mandatory height anomalies as well as their time evolution have been presented for each latitude belt separately. It is important, however, to gain knowledge on the coupling between latitudes. It has been shown that the large-scale features of the leading normal mode for T5C at 20 °S and the large-scale features of the vertically integrated heat source within the TWPWP behave jointly. Also, it is widely known that tropical convection, especially over the TWPWP, acts as a major heat source for general circulation (e.g. Jin and Hoskins, 1995). Such is the importance of this phenomenon that the term Southern Oscillation (SO) (e.g. van Loon and Madden, 1981) has been coined for the inter-annual fluctuations of several variables in the atmosphere as well as in the tropical Pacific Ocean. Likewise, SO extreme phases lead to El Niño or La Niña, although El Niño/Southern Oscillation (ENSO) is the name used in the literature for the interactions between the tropical Pacific Ocean and the atmosphere, disregarding the phase the system is in. Perhaps, ENSO has become the most studied topic in the last decades because it is a major source of variability for the world climate. Notwithstanding, we will not go further into these subject because it is beyond the scope of the present work. Besides, the climatology presented here is not affected by the different phases of ENSO because warm, cold and neutral conditions are equally included in the 35 years spanned by the datasets. Please refer to Wang (2002); McPhaden *et al*. (1998) and references therein, and Neelin *et al*. (1998) and references therein for details on this subject. Undoubtedly, the world climate is driven by the seasonality of the tropical convection, and the purpose from now on is to assess whether these known facts echo in the coupling between the tropopause and the two mandatory levels analysed in this research for latitudes beyond 20 °S under the light of the results presented in the previous section. To do so, the scores are correlated to each other in order to get significant couplings. It is well known that the statistic $t = r\sqrt{n-2}/\sqrt{1-r^2}$ follows a Student distribution with $n-2$ degrees of freedom, n being the sample size and r being the Pearson correlation coefficient. Table V shows the Pearson correlation coefficients between the scores. Only those scores that have significant leading cycles are discussed. Furthermore, only those correlation values marked with an asterisk in Table V are considered. Before analysing the results shown in Table V, it is worth noting that the Pearson coefficient is not robust because strong, but nonlinear, relationships between the pair of variables correlated may not be recognized (see, e.g. Wilks, 2006). Following this, Table V reflects strictly linear relationships. Having noted this important warning, it is surprising that at a glance all correlations to be discussed are positive, indicating

Table V. Correlation matrix for the first two scores (FSs).

			20 °S				30 °S				45 °S			
			T5C		T1C		T5C		T1C		T5C		T1C	
			FS1	**FS2**	FS1	**FS2**	**FS1**	**FS2**	**FS1**	**FS2**	**FS1**	FS2	**FS1**	**FS2**
20 °S	T5C	**FS1**			**0.27**	**0.53***	**0.49**	**0.45**	**0.12**	**0.25**	**0.22**	0.09	**0.44**	**−0.31**
		FS2			**−0.67***	**0.11**	0.05	**−0.26**	**0.12**	**0.13**	**−0.16**	**−0.16**	**−0.28**	0.10
	T1C	FS1					0.09	**0.26**	**−0.13**	**0.27**	**0.11**	0.10	**0.22**	−0.09
		FS2					**0.48**	**0.12**	**0.38**	**0.24**	**0.30**	**−0.11**	**0.36**	**−0.10**
30 °S	T5C	**FS1**							**0.78***	**0.14**	**0.58***	−0.06	**0.61***	0.08
		FS2							**−0.42**	0.08	0.09	**0.22**	**0.34**	**−0.40**
	T1C	**FS1**									**0.56***	**−0.16**	**0.46**	**0.33**
		FS2									−0.03	**−0.16**	−0.05	**−0.17**
45 °S	T5C	**FS1**											**0.84***	**0.33**
		FS2											0.04	**0.24**
	T1C	**FS1**												
		FS2												

Bold face correlation values indicate significance (confidence level set to 95%). Highlighted scores indicate a significant leading cycle (see text). An asterisk indicates values greater than a half, i.e. that the correlation holds for at least 25% of the time, or three months a year, not necessarily consecutive. Redundant information is hidden.

that the correlated pair of variables is climatologically in phase. Moreover, the leading harmonic for all considered time series corresponds to a semi-annual wave. Firstly, same latitude band correlations are discussed. Significant correlation within 20 °S occurs between T5C FS1 and T1C FS2. Seeing that T5C FS1 is supposedly driven by the condensational heating seasonality, the influence this physical process has upon the T1C FS2 variability accounts for at least 28% (this arises from the square of the correlation coefficient). This relationship is evident from ERA-40s' Figure D32 (ERAD32 henceforth) as it shows that diabatic heating sinks in the middle atmosphere are well correlated with diabatic heating sources in UTLS, except during SH summer. The partial correlation for SH summer is not shown here; nevertheless, it can be guessed as being broadly negative to comply with the aforementioned results. Within 30 °S, T5C FS1 and T1C FS1 are strongly correlated, indicating that the percentage of deterministic linear relationship between them is 61%. Finally, within 45 °S, T5C FS1 is strikingly 71% linearly related with T1C FS1. Comparing the (linear) deterministic relationship between T5C FS1 and T1C FS1 for the two latter latitudes, it is worth noting that it increases southwards.

So far, higher correlation values have been discussed only for same latitude bands. Notwithstanding, the (linear) deterministic relationship between 30 °S T5C FS1 and 45 °S T5C FS1 (T1C FS1) is close to 34% (37%). In plain words, at least the third part of the coupling between these two latitudes for the aforementioned variables is deterministic. It is well known that many of the processes in the atmosphere are non-linear (see, e.g. Elsner and Tsonis, 1992; Tsonis and Elsner, 1989), a fact that is reflected in the low- and non-significant correlation coefficients in Table V. These non-linear relationships are yet to be investigated. Likewise, it is important to emphasize that the efforts in trying to explain the foregoing results for the time evolution of the tropopause/mandatory levels coupling as obtained by the EOF analysis as well as the significant linear relationships portrayed in Table V are not explored in the present paper. That the semi-annual wave is embedded in the time series concerned with the discussion of the aforementioned significant correlations is not only a consequence of having subtracted the annual wave from these time series but is also due to the widely known semi-annual oscillation (SAO) signal present in the tropical (van Loon and Jenne, 1969) and extra-tropical (Meehl, 1991) troposphere as well as in upper layers of the atmosphere (e.g. Hamilton, 1986; Kochanski, 1972). An interesting feature tied to the tropical stratospheric SAO is that vertical propagation of planetary waves is inhibited when easterly or very intense westerly winds are present, while the converse of this criterion establishes that vertical propagation is enabled when moderate-to-weak westerlies prevail (Charney and Drazin, 1961). The vertical propagation condition can be generalized to any latitude, therefore vertical waves are trapped unless moderate-to-weak easterly winds are present. Naturally, the weaker the easterly winds, the lesser is the vertical penetration of the upward propagating wave also.

Van Loon and Jenne (1969) present the evolution of zonal geostrophic wind throughout the year for several latitudes in the SH. A SAO signal is embedded in most of these time series and, most importantly, most of the time series at latitudes considered in the above-mentioned paper are quite in phase with the ones corresponding to the scores considered here. Following this, the vertical propagation of planetary waves can be invoked in an attempt to explain the significant correlations portrayed in Table V. ERA-40's Figure D29 presents the world-wide vertical field of zonally averaged geostrophic wind from 1 to 1000 hPa. According to this figure, vertical propagation is enabled (disabled) throughout the troposphere (stratosphere) all year long at 20 °S, although it borders no vertical propagation at all during summer. Except for winter, vertical propagation at 30 °S is enabled in the troposphere. By contrast, during winter, a jet-like locus is present in the vicinities of 200 hPa, and vertical propagation is therefore impossible. With regard to the stratosphere at this latitude, vertical propagation is only possible during winter. With regard to 45 °S, vertical propagation is enabled in the troposphere all year long, whereas in the stratosphere it is prevented during the solstices.

As mentioned, the troposphere-stratosphere system in 20 °S borders no vertical propagation conditions during summer, and recalling that this implies an evanescent wave the situation depicted by T5C EOF1 during this season may be regarded as a trapped wave that contributes to diabatic heating through dissipation, therefore making T5T values positive. Under these assumptions, T5C FS1 is well correlated to T1C FS2 as seen from the prevailing anti-correlation relationships between tropospheric and stratospheric heating rates (cf. ERAD32). Except for winter, vertical propagation is possible throughout the 30 °S troposphere and UTLS, and the propagating wave raises the tropopause as well as both mandatory level surfaces. Anomalies of like sign are thus well depicted for the equinoxes, although this is no longer an acceptable explanation during early summer, when for T5C as well as T1C EOF1 is in indirect mode (negative anomalies) though vertical propagation is still allowed. On the other hand, when vertical propagation is suppressed the signal of diabatic heating -owing to the presence of a trapped wave- appears in EOF2, highlighting the fact that this is a second order effect at this latitude. The model fits reasonably well at 45 °S, as vertical propagation is enabled in the stratosphere only during the equinoxes. Unlike the situation depicted for 30 °S, the effects of diabatic heating due to trapped waves are absent in EOF2, presumably appearing in higher order EOFs not considered here. The linkages between 30 °S and 45 °S can be interpreted the same way as outlined above. It should be noted that these conclusions were drawn based solely on zonally-averaged geostrophic winds, thus disregarding local and regional processes, which also seem to play an important role (e.g. Canziani and Legnani, 2003).

Acknowledgements

First, the authors wish to thank the Department of Atmospheric Science, College of Engineering, University of Wyoming, for their generosity in making their global radiosonde database available to the public domain through http://weather.uwyo.edu/. The lead author wishes to extend his gratitude to the Consejo Nacional de Investigaciones Científicas y Técnicas (CONICET), Argentina, for funding his ongoing Ph.D. grant. Thanks are also due to Prof. Andrew Comrie and two anonymous reviewers for their constructive critics that helped improve this manuscript in many ways. This paper was partially funded by BID1728/OC-AR PICT26094 and CONICET PIP 5276 grants.

References

Appenzeller C, Davies HC. 1992. Structure of stratospheric intrusions into the troposphere. *Nature* **358**: 570–572.

Appenzeller C, Davies HC, Norton WA. 1996. Fragmentation of stratospheric intrusions. *Journal of Geophysical Research* **101**(D1): 1435–1456.

Barry RG, Carleton AM. 2001. *Synoptic and Dynamic Climatology*, Routledge, London, 620 pp.

Baray J-L, Daniel V, Ancellet G, Legras B. 2000. Planetary-scale tropopause folds in the southern subtropics. *Geophysical Research Letters* **27**(3): 353–356.

Berbery EH, Vera CS. 1996. Characteristics of the southern hemisphere winter storm track with filtered and unfiltered data. *Journal of the Atmospheric Sciences* **53**(3): 468–481.

Berrisford P, Hoskins BJ, Tyrlis E. 2007. Blocking and Rossby wave breaking on the dynamical tropopause in the southern hemisphere. *Journal of the Atmospheric Sciences* **64**: 2881–2898. DOI:10.1175/JAS3984.1.

Bischoff SB, Canziani PO, Yuchechen AE. 2007. The tropopause at southern extratropical latitudes: Argentine operational rawinsonde climatology. *International Journal of Climatology* **27**(2): 189–209. DOI:10.1002/joc.1385.

Bradshaw NG, Vaughan G, Ancellet G. 2002. Generation of layering in the lower stratosphere by a breaking Rossby wave. *Journal of Geophysical Research* **107**(D2): 4011. DOI:10.1029/2001JD000432.

Brunet G. 1994. Empirical normal-mode analysis of atmospheric data. *Journal of the Atmospheric Sciences* **51**(7): 932–952.

Bush ABG, Peltier WR. 1994. Tropopause folds and synoptic-scale baroclinic wave life cycles. *Journal of the Atmospheric Sciences* **51**(12): 1581–1604.

Canziani PO, Legnani WE. 2003. Tropospheric-stratospheric coupling: extratropical synoptic systems in the lower stratosphere. *Quarterly Journal of the Royal Meteorological Society* **129**: 2315–2329. DOI:10.1256/qj.01.109.

Canziani PO, Malanca FM, Agosta EA. 2008. Ozone and upper troposphere/lower stratosphere variability and change at southern midlatitudes 1980–2000: decadal variations. *Journal of Geophysical Research* **113**: D20101. DOI:10.1029/2007JD009303.

Charney JG, Drazin PG. 1961. Propagation of planetary-scale disturbances from the lower into the upper atmosphere. *Journal of Geophysical Research* **66**(1): 83–109.

Elsner JB, Tsonis AA. 1992. Nonlinear prediction, chaos, and noise. *Bulletin of the American Meteorological Society* **73**(1): 49–60.

Ertel H. 1942a. Ein neuer hydrodynamischer Wirbelsatz. *Meteorologische Zeitschrift* **59**: 277–281.

Ertel H. 1942b. Ein neuer hydrodynamischer Erhaltungssatz. *Die Naturwissenschaften* **30**: 543–544.

Gates WL. 1961. Static stability measures in the atmosphere. *Journal of Meteorology* **18**: 526–533.

Ghil M, Mo K. 1991. Intraseasonal oscillations in the global atmosphere. Part II: Southern hemisphere. *Journal of the Atmospheric Sciences* **48**(5): 780–790.

Goering MA, Gallus WA, Olsen MA, Stanford JL. 2001. Role of stratospheric air in a severe weather event: analysis of potential vorticity and total ozone. *Journal of Geophysical Research* **106**(D11): 11813–11823.

Golub GH, VanLoan CF. 1989. *Matrix Computations*, 2nd edn. The Johns Hopkins University Press: Baltimore, MD.

Griffiths M, Thorpe AJ, Browning KA. 2000. Convective destabilization by a tropopause fold diagnosed using potential-vorticity inversion. *Quarterly Journal of the Royal Meteorological Society* **126**: 125–144.

Hamilton K. 1986. Dynamics of the stratospheric semiannual oscillation. *Journal of the Meteorological Society of Japan* **64**(2): 227–244.

Hartmann DL. 1977. On potential vorticity and transport in the stratosphere. *Journal of the Atmospheric Sciences* **34**: 968–977.

Haynes P, Scinocca J, Greenslade M. 2001. Formation and maintenance of the extratropical tropopause by baroclinic eddies. *Geophysical Research Letters* **28**(22): 4179–4182.

Hoerling MP, Schaack TK, Lenzen AJ. 1991. Global objective tropopause analysis. *Monthly Weather Review* **119**: 1816–1831.

Hoskins BJ, Hodges KI. 2005. A new perspective on southern hemisphere storm tracks. *Journal of Climate* **18**: 4108–4129.

Inatsu M, Hoskins BJ. 2004. The zonal asymmetry of the southern hemisphere winter storm track. *Journal of Climate* **17**: 4882–4892.

Jin F, Hoskins BJ. 1995. The direct response to tropical heating in a baroclinic atmosphere. *Journal of the Atmospheric Sciences* **52**(3): 307–319.

Johnson RH. 1986. Short-term variations of the tropopause height over the winter MONEX area. *Journal of the Atmospheric Sciences* **43**(11): 1152–1163.

Juckes M. 1994. Quasigeostrophic dynamics of the tropopause. *Journal of the Atmospheric Sciences* **51**(19): 2756–2768.

Kållberg P, Berrisford P, Hoskins B, Simmons A, Uppala S, Lamy-Thépaut S, Hine R. 2005. *ERA-40 Atlas*, *ERA-40 Project Report Series No. 19*, European Centre for Medium Range Weather Forecasts: Shinfield Park, Reading, RG2 9AX, England; viii+191. also available at http://www.ecmwf.int/research/era/ERA-40_Atlas/.

Kidson JW, Sinclair MR. 1995. The influence of persistent anomalies on southern hemisphere storm tracks. *Journal of Climate* **8**: 1938–1950.

Kochanski A. 1972. Semiannual variation at the base of the thermosphere. *Monthly Weather Review* **100**(3): 222–234.

Kowol-Santen J, Ancellet G. 2000. Mesoscale analysis of transport across the subtropical tropopause. *Geophysical Research Letters* **27**(20): 3345–3348.

Kutzbach JE. 1967. Empirical eigenvectors of sea-level pressure, surface temperature and precipitation complexes over North America. *Journal of Applied Meteorology* **6**: 791–802.

Kutzbach JE. 1970. Large-scale features of monthly mean Northern Hemisphere anomaly maps of sea-level pressure. *Monthly Weather Review* **98**(9): 708–816.

Lamarque J-F, Langford AO, Proffitt MH. 1996. Cross-tropopause mixing of ozone through gravity wave breaking: observation and modeling. *Journal of Geophysical Research* **101**(D17): 22969–22976.

Martius O, Schwierz C, Davies HC. 2007. Breaking waves at the tropopause in the wintertime northern hemisphere: climatological analyses of the orientation and the theoretical LC1/2 classification. *Journal of the Atmospheric Sciences* **64**: 2576–2592.

McPhaden MJ, Busalacchi AJ, Cheney R, Donguy J-R, Gage KS, Halpern D, Ji M, Julian P, Meyers G, Mitchum GT, Niiler PP, Picaut J, Reynolds RW, Smith N, Takeuchi K. 1998. The tropical ocean-global atmosphere observing system: a decade of progress. *Journal of Geophysical Research* **103**(C7): 14169–14240.

Meehl GA. 1991. A Reexamination of the mechanism of the semiannual oscillation in the southern hemisphere. *Journal of Climate* **4**: 911–926.

Mo KC, Ghil M. 1987. Statistics and dynamics of persistent anomalies. *Journal of the Atmospheric Sciences* **44**(5): 877–901.

Mote PW, Rosenlof KH, McIntyre ME, Carr ES, Gille JC, Holton JR, Kinnersley JS, Pumphrey HG, Rusell JM III, Waters JW. 1996. An atmospheric tape recorder: the imprint of tropical tropopause temperatures on stratospheric water vapor. *Journal of Geophysical Research* **101**(D2): 3989–4006.

Nakamura H, Shimpo A. 2004. Seasonal variations in the southern hemisphere storm tracks and jet streams as revealed in a reanalysis dataset. *Journal of Climate* **17**: 1828–1844.

Neelin JD, Battisti DS, Hirst AC, Jin F-F, Wakata Y, Yamagata T, Zebiak SE. 1998. ENSO theory. *Journal of Geophysical Research* **103**(C7): 14261–14290.

Newell RE, Gould-Stewart S. 1981. A stratospheric fountain? *Journal of the Atmospheric Sciences* **38**: 2789–2796.

North GR. 1984. Empirical orthogonal functions and normal modes. *Journal of the Atmospheric Sciences* **41**(5): 879–887.

North GR, Bell TL, Cahalan RF, Moeng FJ. 1982. Sampling errors in the estimation of empirical orthogonal functions. *Monthly Weather Review* **110**: 699–706.

Pan LL, Randel WJ, Gary BL, Mahoney MJ, Hintsa EJ. 2004. Definitions and sharpness of the extratropical tropopause: a trace gas perpspective. *Journal of Geophysical Research* **109**: D23103. DOI:10.1029/2004JD004982.

Physick WL. 1981. Winter depression tracks and climatological jet streams in the southern hemisphere during the FGGE year. *Quarterly Journal of the Royal Meteorological Society* **107**: 883–898.

Postel GA, Hitchman MH. 1999. A climatology of Rossby wave breaking along the subtropical tropopause. *Journal of the Atmospheric Sciences* **56**: 359–373.

Poulida O, Dickerson RR, Heymsfield AS. 1996. Stratosphere-tropopshere exchange in a midlatitude mesoscale convective complex, 1, observations. *Journal of Geophysical Research* **101**(D3): 6823–6836.

Price JD, Vaughan G. 1993. The potential for stratosphere-troposphere exchange in cut-off-low systems. *Quarterly Journal of the Royal Meteorological Society* **119**: 343–365.

Quadrelli R, Bretherton CS, Wallace JM. 2005. On sampling errors in empirical orthogonal functions. *Journal of Climate* **18**: 3704–3710.

Reichler T, Dameris M, Sausen R. 2003. Determining the tropopause height from gridded data. *Geophysical Research Letters* **30**(20): 2042, DOI:10.1029/2003GL018240.

Richman MB. 1986. Rotation of principal components. *Journal of Climatology* **6**: 293–335.

Rood RB, Douglass AR, Cerniglia MC, Read WG. 1997. Synoptic-scale mass exchange from troposphere to the stratosphere. *Journal of Geophysical Research* **102**(D19): 23467–23485.

Rotunno R, Skamarock WC, Snyder C. 1994. An analysis of frontogenesis in numerical simulations of baroclinic waves. *Journal of the Atmospheric Sciences* **51**(23): 3373–3398.

Santer BD, Sausen R, Wigley TML, Boyle JS, AchutaRao K, Doutriaux C, Hansen JE, Meehl GA, Roeckner E, Ruedy R, Schmidt G, Taylor KE. 2003. Behavior of tropopause height and atmospheric temperature in models, reanalyses, and observations: decadal changes. *Journal of Geophysical Research* **108**(D1): 4002. DOI:10.1029/2002JD002258.

Schneider T. 2004. The tropopause and the thermal stratification in the extratropics of a dry atmosphere. *Journal of the Atmospheric Sciences* **61**(12): 1317–1340.

Schneider T. 2007. The thermal stratification of the extratropical atmosphere. In *The Global Circulation of the Atmosphere*, Schneider T, Sobel AH (eds). Princeton University Press: Princeton, NJ; 47–77.

Schnur R, Schmitz G, Grieger N, von Storch H. 1993. Normal modes of the atmosphere as estimated by principal oscillation patterns and derived from quasigeostrophic theory. *Journal of the Atmospheric Sciences* **50**(15): 2386–2400.

Seidel DJ, Randel WJ. 2006. Variability and trends in the global tropopause estimated from radiosonde data. *Journal of Geophysical Research* **111**: D21101. DOI:10.1029/2006JD007363.

Seidel DJ, Randel WJ. 2007. Recent widening of the tropical belt: evidence from tropopause observations. *Journal of Geophysical Research* **112**: D20113. DOI:10.1029/2007JD008861.

Seidel DJ, Ross RJ, Angell JK, Reid GC. 2001. Climatological characterisitics of the tropical tropopause as revealed by radiosondes. *Journal of Geophysical Research* **106**(D8): 7857–7878.

Shapiro MA, Hampel T, Krueger AJ. 1987. The Arctic tropopause fold. *Monthly Weather Review* **115**: 444–454.

Shimizu A, Tsuda T. 2000. Variations in tropical tropopause observed with radiosondes in Indonesia. *Geophysical Research Letters* **27**(16): 2541–2544.

Sinclair MR. 1994. An objective cyclone climatology for the southern hemisphere. *Monthly Weather Review* **122**: 2239–2256.

Sinclair MR. 1995. A climatology of cyclogenesis for the southern hemisphere. *Monthly Weather Review* **123**: 1601–1619.

Staley DO. 1960. Evaluation of potential-vorticity changes near the tropopause and the related vertical motions, vertical advection of vorticity, and transfer of radioactive debris from stratosphere to troposphere. *Journal of Meteorology* **17**: 591–620.

Staley DO. 1962. On the mechanism of mass and radioactivity transport from stratosphere to troposphere. *Journal of the Atmospheric Sciences* **19**: 450–467.

Staley DO. 1982. Strontium-90 in surface air an the stratosphere: some interpretations of the 1963–75 data. *Journal of the Atmospheric Sciences* **39**: 1571–1590.

Thuburn J, Craig GC. 1997. GCM tests of theories for the height of the tropopause. *Journal of the Atmospheric Sciences* **54**: 869–882.

Trenberth KE. 1979. Interannual variability of the 500 mb zonal mean flow in the southern hemisphere. *Monthly Weather Review* **107**: 1515–1524.

Trenberth KE. 1980. Planetary waves at 500 mb in the southern hemisphere. *Monthly Weather Review* **108**: 1378–1389.

Trenberth KE. 1981. Observed southern hemisphere eddy statistics at 500 mb: frequency and spatial dependence. *Journal of the Atmospheric Sciences* **38**: 2585–2605.

Trenberth KE. 1982. Seasonality in southern hemisphere eddy statistics at 500 mb. *Journal of the Atmospheric Sciences* **39**: 2507–2520.

Trenberth KE. 1991. Storm tracks in the southern hemisphere. *Journal of the Atmospheric Sciences* **48**(19): 2159–2178.

Tsonis AA, Elsner JB. 1989. Chaos, strange attractors, and weather. *Bulletin of the American Meteorological Society* **70**(1): 14–23.

Uccellini LW, Keyser D, Brill KF, Wash CH. 1985. The President's day cyclone of 18–19 February 1979: influence of upstream trough amplification and associated tropopause folding on rapid cyclogenesis. *Monthly Weather Review* **113**: 962–988.

Vallis GK. 2006. *Atmospheric and Ocean Fluid Dynamics: Fundamentals and Large-Scale Circulation*, Cambridge University Press: Cambridge, UK; 745 pp.

van Loon H, Madden RA. 1981. The southern oscillation. Part I: global associations with pressure and temperature in Northern winter. *Monthly Weather Review* **109**: 1150–1162.

van Loon H, Jenne RL. 1969. The half-yearly oscillations in the tropics of the southern hemisphere. *Journal of the Atmospheric Sciences* **26**: 218–232.

Wallis TWR. 1998. A subset of core stations from the Comprehensive Aerological Reference Dataset (CARDS). *Journal of Climate* **11**: 272–282.

Wang C. 2002. Atmospheric cells associated with El Niño-southern oscillation. *Journal of Climate* **15**: 399–419.

Webster PJ, Lukas R. 1992. TOGA COARE: The coupled ocean–atmosphere response experiment. *Bulletin of the American Meteorological Society* **73**(9): 1377–1416.

Wilks DS. 2006. *Statistical Methods in the Atmospheric Sciences*, 2nd edn. Academic Press: 627.

Wirth V. 2000. Thermal versus dynamical tropopause in upper-tropospheric balanced flow anomalies. *Quarterly Journal of the Royal Meteorological Society* **126**: 299–317.

Wirth V, Egger J. 1999. Diagnosing extratropical synoptic-scale stratosphere-troposphere exchange: a case study. *Quarterly Journal of the Royal Meteorological Society* **125**: 635–655.

World Meteorological Organization (WMO). 1986. Atmospheric ozone 1985: Global ozone research and monitoring report, Rep. No. 16, WMO: Geneva, Switzerland; 392.

World Meteorological Organization (WMO). 1992. *International Meteorological Vocabulary WMO/OMM/BMO – No. 182*, 2nd edn. Secretariat of the World Meteorological Organization: Geneva, Switzerland; 784.

Yanai M, Tomita T. 1998. Seasonal and interannual variability of atmospheric heat sources and moisture sinks as determined from NCEP-NCAR reanalysis. *Journal of Climate* **11**: 463–482.

Zängl G, Hoinka KP. 2001. The tropopause in the polar regions. *Journal of Climate* **14**: 3117–3139.

